Chemosphere 197 (2018) 817–829

Contents lists available at ScienceDirect

Chemosphere

journal homepage: www.elsevier.com/locate/chemosphere

Bimetallic Au-Pd nanoparticles on 2D supported graphitic carbon nitride and reduced graphene oxide sheets: A comparative photocatalytic degradation study of organic pollutants in water

Gitashree Darabdhara [a, b], Manash R. Das [a, b, *]

[a] Advanced Materials Group, Materials Sciences and Technology Division, CSIR-North East Institute of Science and Technology, Jorhat 785006, India
[b] Academy of Scientific and Innovative Research, CSIR-NEIST Campus, India

HIGHLIGHTS

- Bimetallic Au-Pd nanoparticles decorated g-C_3N_4 and rGO nanosheets were developed.
- Degradation of phenolic compounds using Au-Pd/g-C_3N_4 and Au-Pd/rGO was investigated.
- Effect of sunlight, UV light and support material on degradation was studied.
- Factors like pH, catalyst loading, kinetics etc. on photodegradation was examined.
- The photocatalyst displayed excellent reusability and sustainability.

GRAPHICAL ABSTRACT

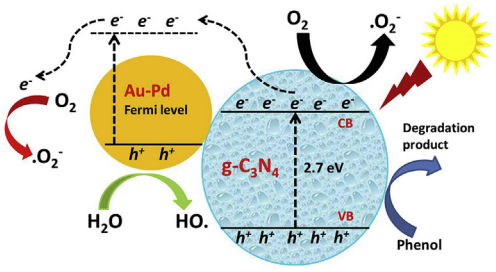

ARTICLE INFO

Article history:
Received 2 September 2017
Received in revised form
13 December 2017
Accepted 15 January 2018
Available online 3 February 2018

Handling Editor: Jun Huang

Keywords:
Au-Pd bimetallic nanoparticle
Graphitic carbon nitride
Reduced graphene oxide
Photocatalytic degradation
Phenolic compound

ABSTRACT

Novel and sustainable bimetallic nanoparticles of Au-Pd on 2D graphitic carbon nitride (g-C_3N_4) and reduced graphene oxide (rGO) sheets was designed adopting an eco-friendly chemical route to obtain Au-Pd/g-C_3N_4 and Au-Pd/rGO, respectively. Elimination of hazardous pollutants, particularly phenol from water is urgent for environment remediation due to its significant carcinogenicity. Considering this aspect, the Au-Pd/g-C_3N_4 and Au-Pd/rGO nanocomposites are used as photocatalyst towards degradation of toxic phenol, 2-chlorophenol (2-CP) and 2-nitrophenol (2-NP) under natural sunlight and UV light irradiation. Au-Pd/g-C_3N_4 nanocomposite exhibited higher activity then Au/g-C_3N_4, Pd/g-C_3N_4 and Au-Pd/rGO nanocomposites with more than 95% degradation in 180 min under sunlight. The obtained degradation efficiency of our materials is better than many other reported photocatalysts. Incorporation of nitrogen atoms in the carbon skeleton of g-C_3N_4 provides much better properties to Au-Pd/g-C_3N_4 nanocomposite than carbon based Au-Pd/rGO leading to its higher degradation efficiency. Due to the presence of these nitrogen atoms and some defects, g-C_3N_4 possesses appealing electrical, chemical and functional properties. Photoluminescence results further revealed the efficient charge separation and delayed recombination of photo-induced electron-hole pairs in the Au-Pd/g-C_3N_4 nanocomposite. Generation of reactive oxygen species during photocatalysis is well explained through photoluminescence study and the sustainability of these photocatalyst was ascertained through reusability study up to eight and five consecutive cycles for Au-Pd/g-C_3N_4 and Au-Pd/rGO nanocomposites, respectively without substantial loss in its activity. Characterization of the photocatalysts after reaction

* Corresponding author. Advanced Materials Group, Materials Sciences and Technology Division, CSIR-North East Institute of Science and Technology, Jorhat 785006, India.
E-mail addresses: mnshrdas@yahoo.com, mrdas@neist.res.in (M.R. Das).

https://doi.org/10.1016/j.chemosphere.2018.01.073

signified the stability of the nanocomposites and added advantage to our developed photocatalytic system.

1. Introduction

With the discovery of the wonder material "graphene" in 2004, it has received widespread attention because of its outstanding properties (Novoselov et al., 2004) and thus is explored in electronics (Lin et al., 2010) and optical devices (Liu et al., 2011), chemical sensors (Deng et al., 2011), energy generation and storage (Liu et al., 2011) etc. Single layer graphene possess sufficient white light absorption capacity accounting to 2.3% by a single layer, 4.6% by bilayer and 11.5% by a five layer thick flake graphene (Nair et al., 2008). The use of graphene as a photocatalytic material started when Akhavan reported graphene oxide platelets on anatase TiO_2 thin films for the photoinactivation of bacteria (Akhavan and Ghaderi, 2009). Since 2010, work on graphene based photocatalyst accelerated. So far, the topic "photocatalysis & graphene" has surpassed over 1000 publications. Until now, graphene based photocatalyst is used towards photocatalytic degradation of pollutants and bacteria, water splitting, reduction of CO_2 etc. (Pawar and Lee, 2014; Zhang et al., 2015).

The discovery of such sensational properties of graphene rejuvenated work on other 2D materials like graphitic carbon nitride (g-C_3N_4), transition metal chalcogenides, hexagonal boron nitrides owing to their fantastic properties and application (Xu et al., 2013; Low et al., 2014).

Recently, g-C_3N_4 has attracted considerable attention as it is the most stable allotrope and possesses layered structure like graphene with chemical compositions of C, N and H and possesses good stability and interesting electronic structure with a band gap of 2.7 eV (Wang et al., 2009). Additionally, it is synthesized from cheap feedstocks like urea, cyanamide etc. and is thus useful in photocatalysis, heterogeneous catalysis and fuel cells (Ren et al., 2014; Wang et al., 2012; Zheng et al., 2012; Tahir et al., 2014). However, its use as photocatalyst is limited by low quantum efficiency, small specific surface area and fast recombination rate of electron hole pairs and thus its surface is modified via deposition of metals like Au (Chen et al., 2014b), Ag (Bai et al., 2014) etc., non-metal like S (Liu et al., 2010), CdS (Ge et al., 2012), semiconductor like $BiWO_6$ (Tian et al., 2013), ZnO (Chen et al., 2014a), $ZnTiO_3$/g-C_3N_4 (Pawar et al., 2017) etc. and preparation of lamellar structured g-C_3N_4 (Yang et al., 2013) to improve its photocatalytic activity. Presence of metallic nanoparticles limits the recombination of photogenerated electrons and prolongs the lifetime of the radicals. Bimetallic nanoparticles consisting of two elements achieve greater potential in catalytic applications then their monometallic counterparts owing to the synergistic effects. A number of bimetallic systems supported on g-C_3N_4 has been synthesized such as AgPd for dehydration of formic acid (Yao et al., 2017), CuAg for hydroxylation of benzene (Verma et al., 2017), CuCo, FeCo, NiCo, CuNi and FeNi for hydrogen evolution from ammonia borane (Zhang et al., 2017a) etc. However, no literature focuses on the use of bimetallic nanoparticles immobilized on g-C_3N_4 towards photocatalytic degradation of harmful organic pollutants. Amongst different bimetallic systems, Au-Pd represents an important catalytic system explored in formic acid dehydrogenation (Mentin et al., 2013), photocatalytic Suzuki coupling reaction (Xiao et al., 2014), phenol photodecomposition (Su et al., 2012), hydrogen evolution reactions (Darabdhara et al., 2015) etc. AuPd nanoparticles supported on other substrates such as AuPd alloy on 2D $BiVO_4$ nanosheets was used as photocatalyst towards degradation of Rhodamine B under visible light (Zhang et al., 2017b). Padilla and co-workers designed AuPd/TiO_2 photocatalyst for degradation of methyl orange dye molecule (Padilla et al., 2017). Likewise, Panigrahy and co-workers designed AuPd nano-alloy ZnO-rGO for the degradation of rhodamine 6G dye with 100% degradation (Panigrahy and Sarma, 2015). Efforts have stemmed for developing AuPd nanoparticles on g-C_3N_4 for energetic and environmental applications. Feng et al. developed AuPd nanoclusters on g-C_3N_4 for enhanced photocatalytic oxygen reduction and hydrogen evolution reactions (Feng et al., 2016). Han's group designed AuPd co-catalyst decorated g-C_3N_4 photocatalyst for high H_2 evolution activity under visible light irradiation (Han et al., 2015a). In another work by Fang, AuPd nanoparticles on g-C_3N_4 quantum dots were found to exhibit excellent catalytic performance towards reduction of *p*-nitrophenol (Fang et al., 2017). So far, there is no report on the use of AuPd on g-C_3N_4 for photocatalytic degradation of carcinogenic organic pollutants.

The escalating use of phenolic compounds in different applications such as a disinfectant, chemical reagent, in production of several industrial compounds etc. has posed a serious environmental hazard (Wu et al., 2008). United States Environment Protection Agency (USEPA) has listed eleven phenolic compounds amongst priority pollutants because of their high toxicity, carcinogenicity, high stability and bioaccumulation property which endanger ecosystems in water bodies and human health (Keith and Telliard, 1979). Thus, an efficient economic treatment for eliminating these toxins is crucial. Because of the high stability of the aromatic rings and the hydrophilicity of the hydroxyl group, phenol has purposed the role of a model pollutant aimed at developing advanced oxidation processes (AOPs) like ozonation (Yamamoto et al., 1979), electrochemical oxidation (Sharifian and Kirk, 1986), photocatalytic oxidation (Wei et al., 1990), H_2O_2 and Fenton treatment (Kang et al., 2002), microwave oxidation (Han et al., 2004) etc. However, these are limited by slow degradation, incomplete removal and high cost and are no longer pertinent to the needs of modern industry (D'Oliveira et al., 1990). Photocatalysis has proven to be a widely accepted AOP technique with great potential in the elimination of phenolic compounds (Turchi and Ollis, 1990). Ever since the pioneering work by Fujisima on "photocatalytic water-splitting on TiO_2 electrodes" widespread researches on semiconductor photocatalytic oxidation of pollutants have aroused (Fujishima and Honda, 1972). Nevertheless, owing to the high band gap and fast recombination of the photogenerated electron-hole pairs, it is necessary to develop new photocatalyst with good charge separation and wide absorption range in the entire spectrum (Ren et al., 2014). TiO_2 microspheres decorated bimetallic nanoparticles (Ag-Au, Ag-Pt, Ag-Pd, Au-Pt, Au-Pd and Pt-Pd) was investigated in phenol degradation process under UV and visible light irradiation (Grabowska et al., 2016). Decahedral TiO_2 decorated with bimetallic nanoparticles (Ag-Pt, Ag-Au, Au-Pd, Au-Pt) was also used for degradation of phenol under UV–visible light irradiation with more than 66% degradation efficiency in 90 min (Diak et al., 2017). TiO_2 modified with Au-Pd nanoparticles was prepared using a water-in-oil microemulsion system by calcination from 350 to 700 °C and their photocatalytic activity was evaluated under visible and UV light. Their study showed that Au-Pd/TiO_2

samples calcinated at 350 and 400 °C possess the highest photocatalytic activity when degrading phenol under visible light, which is more than 4 times that of calcinated at 450 °C (Cybula et al., 2014). Although all the nanocomposites exhibited good photocatalytic degradation efficiency, none of the studies focused on the sustainability and stability of the nanocomposites.

Bimetallic Au and Pd on g-C_3N_4 and graphene can serve the role of a model photocatalyst for the removal of phenol from water due to the strong surface plasmon properties of the noble metals as well as visible light absorbing capacity of g-C_3N_4 and also due to the presence of high electron density on graphene. Considering these properties and the need for developing efficient, sustainable and stable photocatalyst, we herein report the synthesis of bimetallic Au-Pd nanoparticles on g-C_3N_4 and rGO by an eco-friendly and an easy solution chemistry technique. All characterizations concerning rGO and Au-Pd/rGO nanocomposites are provided in our previously published paper (Darabdhara et al., 2016). In the current manuscript, we have reported the synthesis of Au-Pd nanoparticles on g-C_3N_4 by a similar process as adopted for the synthesis of Au-Pd/rGO nanocomposites. Only the photocatalytic degradation activity of Au-Pd/g-C_3N_4 nanocomposites towards phenolic compounds is compared to that of previously reported Au-Pd/rGO nanocomposites to establish the influence of different 2D support material on photocatalytic degradation studies. The materials are characterized by high resolution transmission electron microscopy (HRTEM) equipped with energy dispersive X-ray (EDX), field emission scanning electron microscopy (FESEM), powder X-ray diffraction (PXRD), diffuse reflectance infrared Fourier transform (DRIFT), atomic force microscopy (AFM), thermal gravimetric analysis (TGA) and zetasizer. For the first time, Au-Pd/g-C_3N_4 and Au-Pd/rGO nanocomposites are reported as active photocatalyst towards degradation of phenol, 2-CP and 2-NP under various conditions. The efficiency of degradation in presence of sunlight and UV light was evaluated. The role of the support material in degradation of phenol was emphasized by comparing the activity of Au-Pd on g-C_3N_4 and graphene. The generation of primary reactive species i.e. hydroxyl radicals responsible for photocatalytic decomposition of phenol was studied with the help of photoluminescence study and details photocatalytic mechanism is established. We also successfully determined the sustainability and stability of the photocatalyst by studying the reusability up to eight and five consecutive cycles for Au-Pd/g-C_3N_4 and Au-Pd/rGO nanocomposites, respectively without substantial loss in its activity. Characterization of the photocatalyst after reaction indicated no significant change in the size, crystallinity and surface morphology thus assuring the sustainability of the nanocomposites. Since both our support materials g-C_3N_4 and rGO are prepared from cheap feedstocks and also since the activity of our photocatalyst is excellent even after photocatalytic reaction, we can claim that our material is sustainable and can compete with other photocatalyst towards degradation of toxic environmental pollutants.

2. Experimental

2.1. Materials

Gold (III) chloride trihydrate (Sigma Aldrich, Germany), palladium (II) chloride (99.9%, Alfa Aesar, UK), L-ascorbic acid (Sigma Aldrich, Germany), urea (Sigma Aldrich, Germany), phenol (Alfa Aesar, UK), 2-nitrophenol (Alfa Aesar, UK), 2-chlorophenol (Alfa Aesar, UK) were used as received.

2.2. Synthesis of Au-Pd/g-C_3N_4 nanocomposite

The precursor urea (15 g) was taken in a silica crucible and calcinated at 550 °C for 3 h at a ramping heat of 5 °C min^{-1}. The yellow product obtained was ultrasonicated in deionized (DI) water to get g-C_3N_4 with a concentration of 10 mg mL^{-1}. Above g-C_3N_4 solution (10 mL) was mixed with aqueous $HAuCl_4$ (1 mM) and $PdCl_2$ (3 mM) and stirred for 20 min followed by addition of ascorbic acid. Entire solution was stirred for 2 h at 85 °C, cooled and filtered followed by washing with water and ethanol and dried at 65 °C to obtain Au-Pd/g-C_3N_4 nanocomposite. Similarly, monometallic Au/g-C_3N_4 and Pd/g-C_3N_4 nanocomposites were synthesized by mixing g-C_3N_4 solution with either aqueous $HAuCl_4$ or $PdCl_2$ solutions. The concentrations of the monometallic precursors and the reducing agents were kept the same as in bimetallic Au-Pd/g-C_3N_4 nanocomposite.

2.3. Preparation of Au/rGO, Pd/rGO and Au-Pd/rGO nanocomposites

Au/rGO, Pd/rGO and Au-Pd/rGO nanocomposites were synthesized as discussed in our publication (Darabdhara et al., 2016).

2.4. Characterization technique

Scanning electron microscope images were recorded in scanning electron microscope (FESEM, Zeiss Gemini, Germany) at an accelerating voltage of 9-7 kV. X-ray powder diffraction (XRD) was recorded in a Rigaku X-ray diffractometer that operated at a scanning rate of 3°/min from 5 to 100° and uses a X-ray source consisting of Cu Kα that emits X-ray wavelength of, $\lambda = 1.54056$ Å at a generator voltage of 40 kV and current of 40 mA (model: ULTIMA IV, Rigaku, Japan). The crystal structure and morphology were characterized by transmission electron microscopy (TEM), high-resolution TEM (HRTEM) and energy dispersive X-ray (EDX) spectra using a JEOL JEM 2100, transmission electron microscope (Japan) operating at an accelerating voltage of 200 kV. Herein, dispersed colloidal solutions of nanocomposites were prepared and drop casted onto standard carbon-coated copper grids which were then air dried at room temperature. Diffuse reflectance infrared Fourier transform (DRIFT) spectra were noted in an IR Affinity-1 FT-IR spectrophotometer equipped with a Shimadzu DRS-8000 DRIFT accessory working in the range of 400–4000 cm^{-1}. Thermogravimetric analysis (TGA) of the sample was recorded using TA-SDT (model: Q600DT, TA instrument, USA) at an increasing temperature rate of 5 °C/min. Room temperature photoluminescence (PL) spectra of the photocatalyst was obtained using a fluorescence spectrophotometer Horiba Instruments Inc. Edison, NJ USA equipped with a 150 W ozone free vertically mounted xenon arc lamp and connected with FluorEssence software at an excitation wavelength of 325 nm. Atomic force microscopy (AFM) images were recorded in a Nanomagnetic hpm microscope operating in the dynamic mode at room temperature. Maximum scan area for the AFM analysis is chosen as 20 μm × 20 μm and the image size is taken as 256 × 256 pixels. A UV–visible spectrophotometer, Shimazdu, Japan was used for monitoring the photocatalytic activity of the catalyst. The initial and the final products in the 2-CP and 2-NP degradation were analysed using ion chromatography (IC) (Metrohm Compact IC Pro 882, Switzerland). Anion chromatography analysis was carried out for the two phenol molecules before and after degradation under sunlight irradiation. Zeta potential measurements of Au-Pd/g-C_3N_4 and Au-Pd/rGO nanocomposites were recorded in a Zetasizer (Nano ZS, Malvern, UK) at room temperature in the wider pH range.

2.5. Photocatalytic activity

Degradation was studied by irradiating aqueous phenolic suspensions containing the catalyst under sunlight and UV-light.

Sunlight irradiated photocatalysis were carried out on bright sunny days between 10 a.m. and 2 p.m. with an average sunlight intensity of 600–900 W/m^2 (measured by solar power meter, KM SPM 11). The UV light experiments were carried out with a low pressure UV lamp of wavelength 254 nm and 125 W. Typically, a desired amount of photocatalyst was added to 30 mL aqueous organic pollutants and mechanically stirred and exposed to sunlight and UV light for fixed time periods. At fixed time intervals, 2 mL reaction mixture was taken out with a micro syringe and the catalyst separated using a polytetrafluoroethylene (PTFE) membrane. The remaining phenolic concentration was determined by monitoring the filtrate using a UV–visible spectrophotometer. Degradation rate of phenol is expressed as

$$D = (C_o - C_t)/C_o \times 100\%$$

where, C_o and C_t are the concentrations of phenol in the initial sample and final sample, respectively. Blank experiments containing phenol solutions in absence of photocatalyst were also executed.

3. Results and discussions

3.1. Characterization of nanocomposite materials

The XRD pattern (Fig. 1A) for g-C_3N_4 exhibits two distinct peaks corresponding to (100) and (002) planes at 2θ value 13.04° and 27.38°, respectively (Han et al., 2015b). For Au-Pd/g-C_3N_4 nanocomposite, diffractions at 2θ value of 39.24°, 45.60°, 66.66° and 80.32° corresponds to (111), (200), (220) and (311) plane of *fcc* Au-Pd/g-C_3N_4. For Au/g-C_3N_4, diffractions at 38.02°, 44.20°, 64.48°, 77.52° and 81.64° corresponds to (111), (200), (220), (311) and (222) planes of *fcc* Au. For Pd/g-C_3N_4, diffractions at 39.90°, 46.42°, 67.92° and 81.90° corresponds to (111), (200), (220) and (311) plane of *fcc* Pd. For Au-Pd/g-C_3N_4 nanocomposite, the diffractions are located between those of Au/g-C_3N_4 and Pd/g-C_3N_4 thus confirming the alloy nature of the nanocomposite. For all the nanocomposites, another peak at 27.44° is due to the presence of (002) plane of g-C_3N_4. For efficient photocatalytic efficiency, the separation of photogenerated electron-holes is a key factor and this separation efficiency can be studied with the help of photoluminescence (PL) spectra of both the pure g-C_3N_4 and hybrid catalyst. The PL spectra

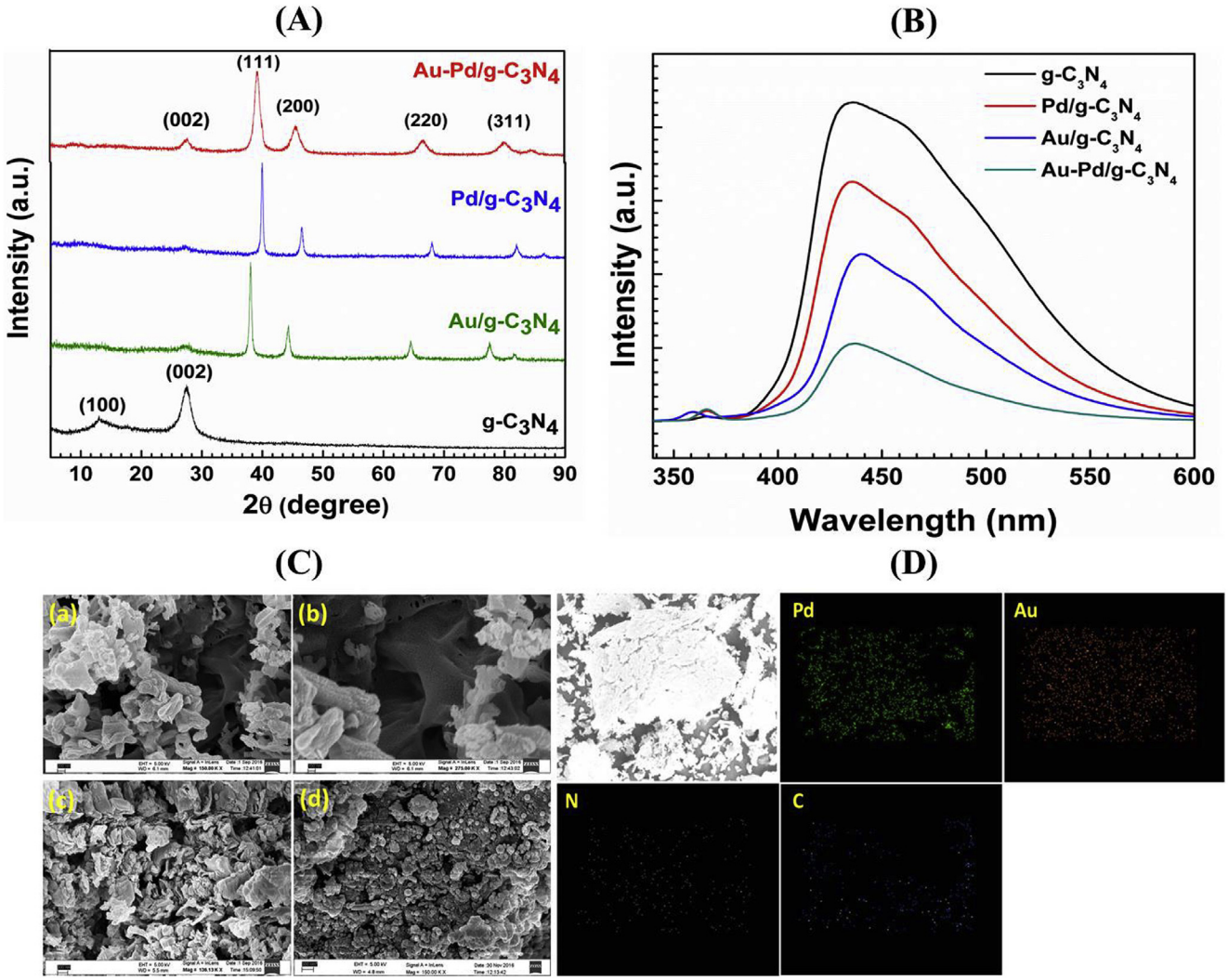

Fig. 1. (A) XRD pattern (B) PL spectra of g-C_3N_4, Au/g-C_3N_4, Pd/g-C_3N_4 and Au-Pd/g-C_3N_4 nanocomposites (C) FESEM images of g-C_3N_4 (a,b) and Au-Pd/g-C_3N_4 (c,d) and (D) corresponding elemental mapping.

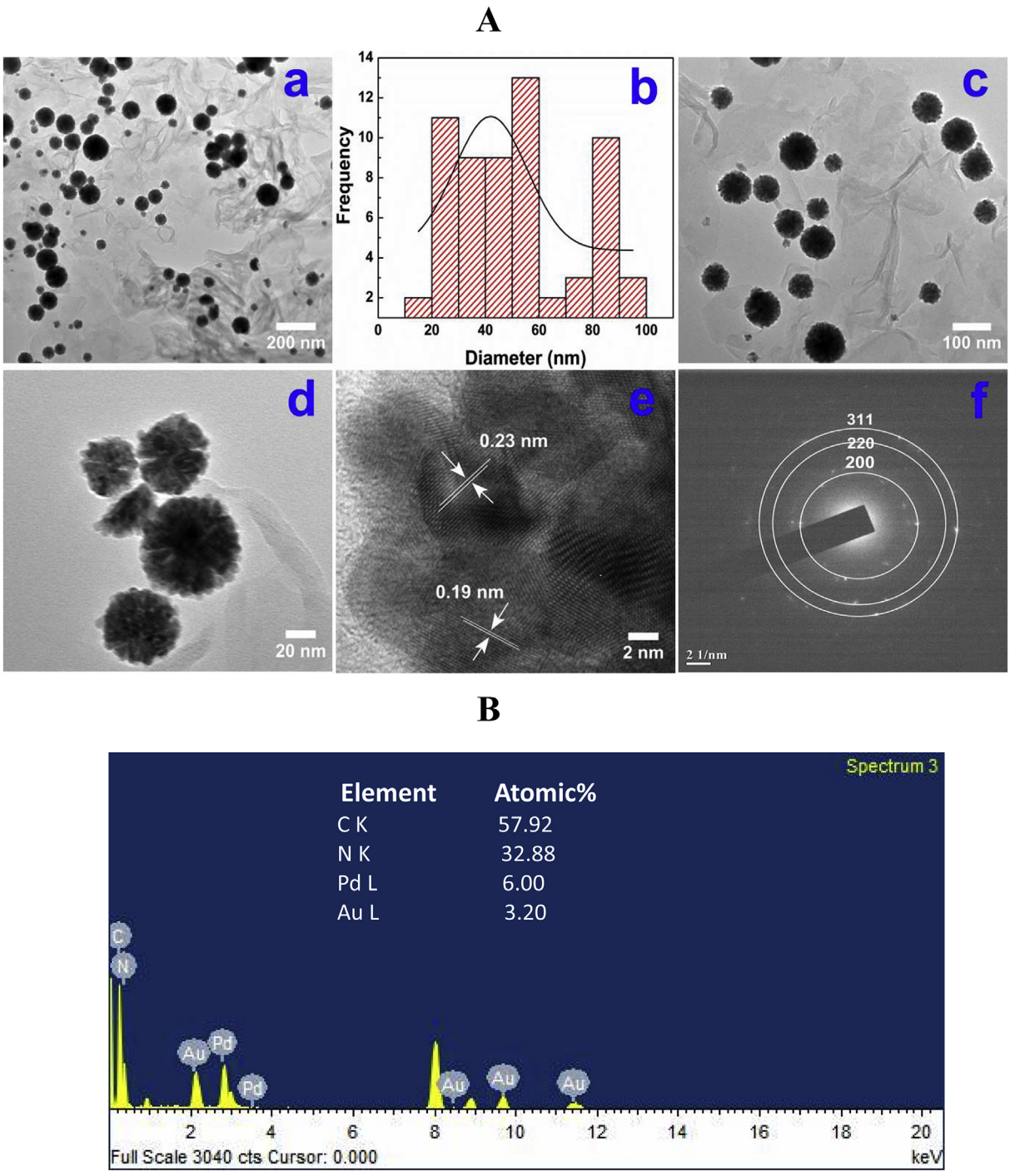

Fig. 2. (A) Low resolution TEM images (a); Size distribution (b); medium magnification TEM image (c,d); HRTEM (e); SAED pattern (f) of Au-Pd/g-C_3N_4 nanocomposite **(B)** EDX analysis of Au-Pd/g-C_3N_4 nanocomposite.

provide information on detecting the charge separation, migration, transfer and recombination processes of photogenerated electron hole pairs in semiconductors. As the PL spectra is derived from the recombination of free carriers, weaker the PL intensity higher is the separation probability or lower the recombination process of the photogenerated charge carriers. Higher the PL intensity, faster the recombination processes of photogenerated charge carriers. The PL spectra (Fig. 1B) recorded at room temperature with an excitation wavelength of 325 nm for pure g-C_3N_4 and its composites displays an emission peak centered at 436 nm which is attributed to the n-π^* electronic transition (Pawar et al., 2014). From Fig. 1B it is seen that pure g-C_3N_4 exhibits PL spectra with highest intensity indicating highest recombination rate of the photoelectrons that generally leads to reduced photocatalytic activity. However, quenching in the PL intensity is observed in the case of the composite material which is most significant in case of Au-Pd/g-C_3N_4 nanocomposite. This weak intensity in the PL signal of Au-Pd/g-C_3N_4 nanocomposite in comparison to other composite materials indicates lower recombination of the photogenerated electrons. Thus, doping g-C_3N_4 with bimetallic Au and Pd nanoparticles can

successfully inhibit recombination rate of the photogenerated electrons leading to enhanced photocatalytic activity. FESEM shows the surface morphology of g-C_3N_4 and Au-Pd/g-C_3N_4. Fig. 1C (a,b) shows the presence of irregularly curved layers of g-C_3N_4. For Au-Pd/g-C_3N_4, small and spherical Au-Pd particles are seen on the surface of g-C_3N_4 (Fig. 1C (c,d)). The corresponding mapping analysis (Fig. 1D) confirms the coexistence of bimetallic Au and Pd on the surface of g-C_3N_4. The identification of Au and Pd in the mapping analysis along with C and N confirms the formation of bimetallic nanoparticles which was further authenticated by the TEM-EDX spectra (Fig. 2B). The FESEM images of the monometallic Au and Pd nanocomposites are presented in Fig. S1 of the Supporting Information (SI).

Low resolution TEM images of Au-Pd/g-C_3N_4 (Fig. 2A (a)) shows the presence of spherical nanocrystals of bimetallic Au-Pd on exfoliated thin nanosheets of g-C_3N_4. The average particle size of the nanoparticles was found to be 41.9 ± 8.29 nm as shown in Fig. 2A (b). Medium magnification TEM (Fig. 2A (c)) shows the formation of nanoparticles in the form of flower. The crystallinity and alloy nature is reflected from the HRTEM images (Fig. 2A (d)). Lattice fringes corresponding to the (111) planes of Au with an interplanar spacing of 0.23 nm and (200) planes of Pd *fcc* structures with an interplanar spacing of 0.19 nm is seen in Fig. 2A (e). The selected area electron diffraction (SAED) pattern (Fig. 2A (f)) confirms the polycrystalline nature. The bright spots correspond to the *fcc* crystal planes. The Au-Pd nanoparticles synthesized on rGO sheets exhibited an average size of 37 ± 0.6 nm as discussed in literature. It is observed that there is size variation of the nanoparticles depending on the use of the support material. However, the variation is not significant and thus we can remark that the size and shape of Au-Pd nanoparticles is not much dependent on the support material. The detailed TEM images of the monometallic Pd/g-C_3N_4 and Au/g-C_3N_4 are provided in the SI (Fig. S2).

The corresponding EDX of Au-Pd/g-C_3N_4 nanocomposites is presented in Fig. 2B. The EDX analysis gives evidence for the co-existence of Au and Pd in Au-Pd/g-C_3N_4. The Au-Pd/g-C_3N_4 nanocomposite contains around 57.92 atomic% of C, 32.88 atomic% of N, 6.00 atomic% of Pd and 3.20 atomic% of Au as obtained from EDX analysis.

DRIFT spectra of g-C_3N_4 and Au-Pd/g-C_3N_4 (Fig. S3a) shows the characteristics vibration modes of typical g-C_3N_4. Details are furnished in the SI. Thermogravimetric analysis (TGA) of the nanocomposite (Fig. S3b) was carried out from room temperature to 1000 °C at a heating rate of 20 °C min^{-1}. Details thermal properties are explained in the SI.

The morphology of Au-Pd/g-C_3N_4 was further analysed with the help of AFM images. The AFM images are provided in Fig. S4. The AFM analysis reveals highly symmetrical particles of Au-Pd.

Stability of the colloidal suspensions of Au-Pd/g-C_3N_4 nanocomposite was ascertained with the help of zeta potential measurements in a wider pH range from 2 to 12. The zeta potential of all the nanocomposites Au-Pd/g-C_3N_4, Au/g-C_3N_4, Pd/g-C_3N_4 and g-C_3N_4 is shown in Fig. S5. The zeta potential of bare g-C_3N_4 is found to be 25.96 mV at pH 2 which decreases to −32.26 mV at pH 12. The isoelectric point (IEP) for bare g-C_3N_4 is found at pH 4.07. For Au/g-C_3N_4, the zeta potential at pH 2 is found to be 11.4 which decrease to −30.9 mV at pH 12. Similarly for Pd/g-C_3N_4, the surface charge at pH 2 is found to be 2.31 which decrease to −12.5 mV at pH 12. For both Au/g-C_3N_4 and Pd/g-C_3N_4, the IEP is found to decrease in comparison to bare g-C_3N_4 and are obtained at 3.92 and 3.72

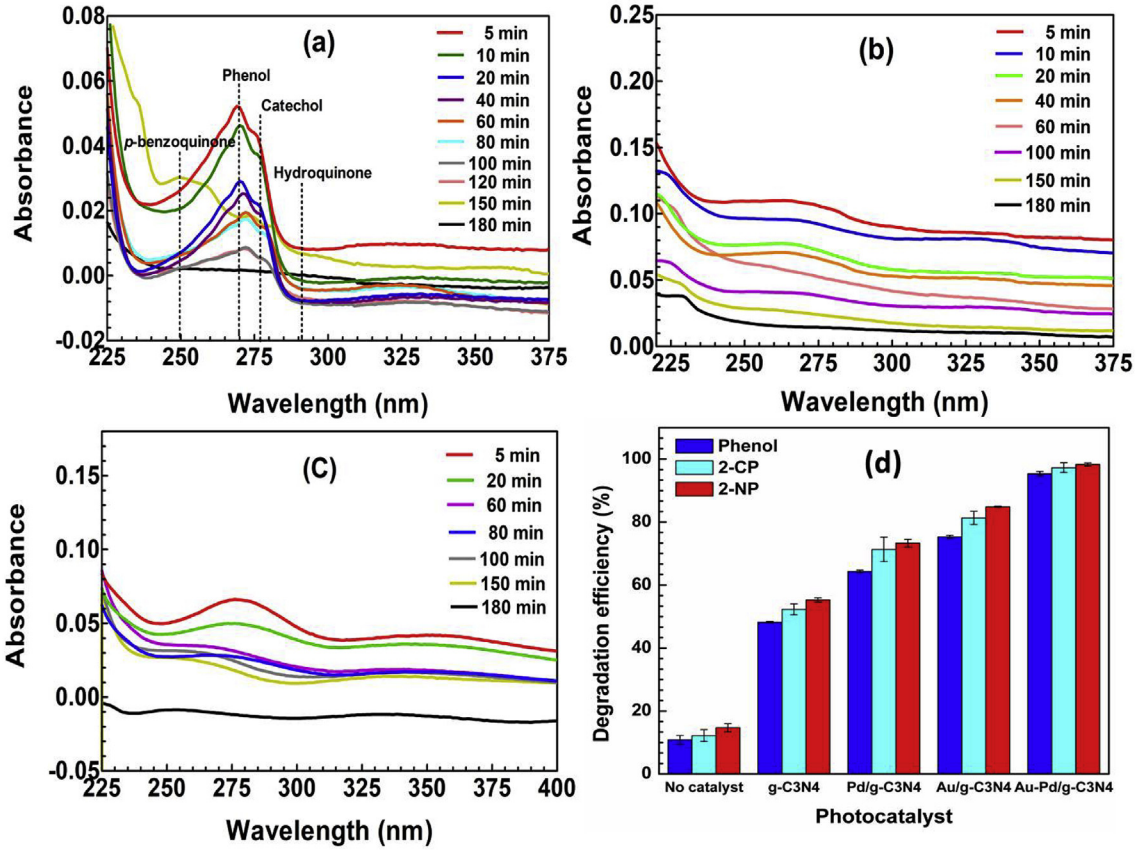

Fig. 3. UV–visible absorbance spectra of (a) phenol (b) 2-CP and (c) 2-NP in presence of Au-Pd/g-C_3N_4 nanocomposite (d) Degradation of phenol, 2-CP and 2-NP in presence of Au/g-C_3N_4, Pd/g-C_3N_4, Au-Pd/g-C_3N_4 nanocomposites and also in absence of photocatalyst at pH 7, 0.5 mM phenol concentration and catalyst loading of 0.5 gL^{-1}

respectively. For bimetallic Au-Pd/g-C_3N_4, surface charge at pH 2 is found at 2.2 mV and decreases to −21.2 mV at pH 12. Also, the IEP for bimetallic Au-Pd/g-C_3N_4 nanocomposite the IEP is found to further decrease to pH 2.37. The lowering of the zeta potential of the nanocomposites is probably due to the adsorption of negatively charged counter-ions, i.e. Cl^- ions from the metal precursors during synthesis. Moreover, the presence of low amounts of g-C_3N_4 in the nanocomposites may also be a reason for the lowering of the zeta potential in the nanocomposites in than in the case of bare g-C_3N_4 (Fageria et al., 2016).

3.2. Photocatalytic activity

For photocatalysis, initially a test for adsorption of phenol prior to exposure of either sunlight or UV light was carried out in dark for 1 h to obtain the adsorption-desorption equilibrium. No significant adsorption was obtained. This was followed by exposing the phenolic solutions to either sunlight or UV light under suitable conditions. Aliquots of reaction mixture were withdrawn at fixed time and monitored using a UV–visible spectrophotometer. The photodegradation profile of phenol, 2-CP and 2-NP in sunlight is shown in Fig. 3a-c. Under sunlight, 95.3% phenol, 97.3% 2-CP and 98.3% 2-NP degradation was achieved in 180 min. Phenol exhibits a characteristics peak at 273 nm which gradually decreases on exposure to sunlight. During photocatalysis, phenols undergo oxidation to produce hydroxy phenols by the oxidizing species produced. The phenol absorbance at 273 nm reduces and other peaks corresponding to catechol (280 nm), hydroquinone (290 nm), *p*-benzoquinone evolve and finally via these intermediates phenols break down to their corresponding acids and ultimately to CO_2 and water.

Comparative degradation portfolio of the phenolic compounds is shown in Fig. 3d. In absence of catalyst very less degradation was obtained. Also, in presence of g-C_3N_4 alone less than 56% degradation efficiency was obtained which was found to increase in presence of Pd/g-C_3N_4 and Au/g-C_3N_4. However, in presence of Au-Pd/g-C_3N_4 nanocomposite, dramatic photodegradation efficiency for all the three phenols was obtained which is attributed to the synergistic effects of Au, Pd and g-C_3N_4 in Au-Pd/g-C_3N_4 nanocomposites. Also the efficiency of Au-Pd/g-C_3N_4 nanocomposite was compared with our reported Au-Pd/rGO nanocomposite. In presence of Au-Pd/rGO nanocomposite phenol degradation was around 94.4% in 300 min whereas that of 2-CP and 2-NP was around 96.7 and 98.6%, respectively in 180 min. However, degradation efficiency of Au-Pd/g-C_3N_4 nanocomposite is relatively higher to that of Au-Pd/rGO nanocomposite. g-C_3N_4 with a band gap of 2.7 eV acts as an attractive visible light photocatalyst. Since around 43% of the available solar energy accounts to visible light and also due of the surface plasmon resonance (SPR) effect, Au is capable of absorbing more visible light so it is observed that Au-Pd/g-C_3N_4 nanocomposite acted as a better catalyst then Au-Pd/rGO nanocomposite towards degradation of phenolic compounds in water. Several reports on the degradation of phenol using composites of g-C_3N_4 are published and provided in Table S1. In

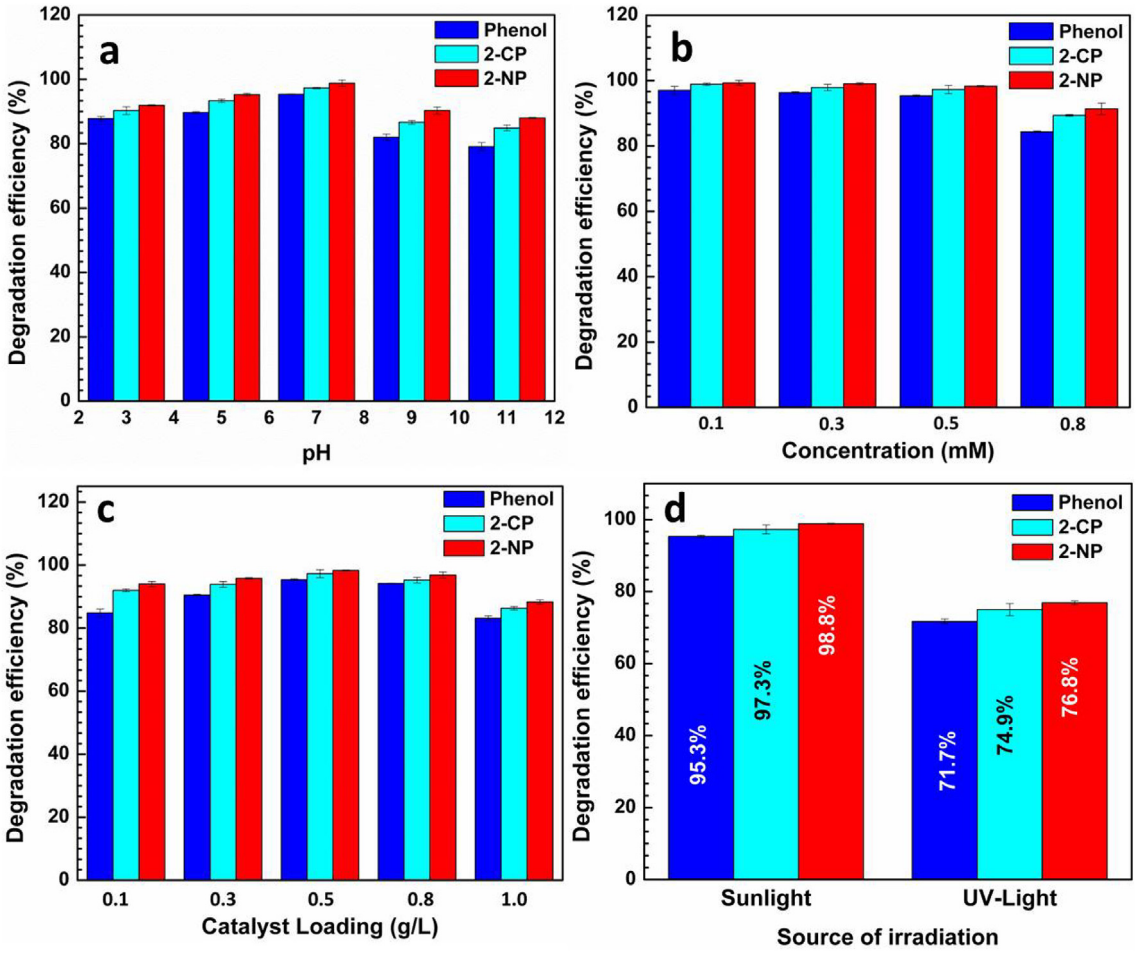

Fig. 4. (a) Degradation of phenolic compounds at different pH (b) At different phenol concentration (c) At different catalyst loading and (d) Comparative degradation profile of phenol, 2-CP and 2-NP using Au-Pd/g-C_3N_4 nanocomposite in presence of sunlight and UV light irradiation.

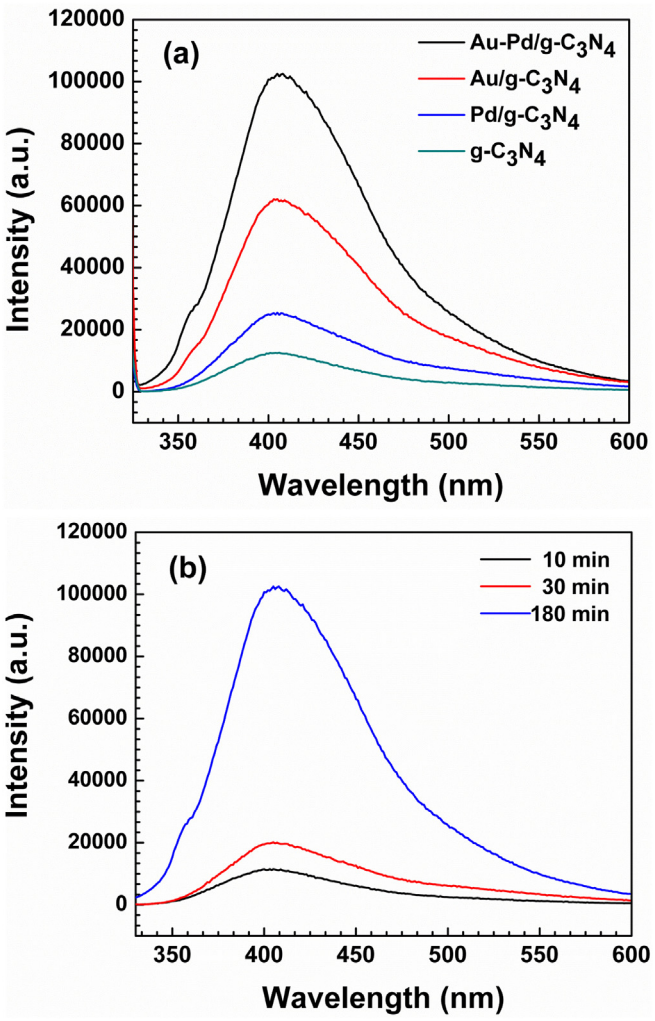

Fig. 5. PL spectra of (a) different catalyst (b) Au-Pd/g-C_3N_4 nanocomposite with time.

comparison, our photocatalyts consisting of Au-Pd/g-C_3N_4 and Au-Pd/rGO demonstrated quite considerable performance towards degradation of phenolic compounds and represents an important class of material with excellent photocatalytic activity.

3.3. *Influence of pH, initial phenol concentration and amount of catalyst*

The pH value influences the active species occurring in the solution and influences the degradation of phenol on the photocatalyst surface. The influence of pH (Fig. 4a) on degradation of phenol follows the trends pH 7 > pH 6 > pH 5 > pH 4 > pH 3 > pH 9 > pH 11. It is observed that a degradation of about 95.3% was obtained for phenol using Au-Pd/g-C_3N_4 nanocomposite at pH 7. The efficiency of degradation is found to be high in neutral medium followed by weak acidic and basic medium. For 2-CP and 2-NP a degradation of 97.3 and 98.3% was obtained, respectively at pH 7 and at 180 min. Thus, optimized pH for all the phenolic compounds is at pH 7. The surface protonation of the photocatalyst, point of zero charge and the dissociation of phenol are all pH dependent. Phenol has a pK_a value of 9.8, below which it exists as a neutral species (C_6H_5OH) and above it as phenoxide ($C_6H_5O^-$) ion (Boukhatem et al., 2017). Fig. 4a clearly represents the dependence of photocatalytic degradation on the pH of the medium. As the pH increases there is a gradual increase of degradation efficiency which is found to be highest in the neutral medium (pH 7) and then again decreases in higher alkaline medium (pH 11). Phenol has a pK_a at 9.8 as mentioned and our most effective photocatalyst Au-Pd/g-C_3N_4 has an IEP at 2.37 (Fig. S5). At low pH, the surface of the photocatalyst is occupied with H^+ ions and thus the generation of •OH radical is slowed down because the excited e^- in the conduction band reacts with H^+ ions and gets neutralized. With increase in pH the surface protonation decreases and at pH 7 most of the phenols are un-dissociated and maximum phenol molecules are adsorbed on the photocatalyst surface and photodegradation rate is enhanced. However, in alkaline medium, the surface of the photocatalyst and the phenol are negatively charged and repel away and as a result the degradation efficiency decreases. Another advantage of our catalytic system is that the industrial effluents are mild to weakly acidic in nature and since our photocatalyst works best in this pH range so it can be effectively used to treat industrial effluents. The degradation efficiency as a function of pH is shown in Fig. S6.

Effect of phenolic concentration was evaluated for concentrations 0.1, 0.3, 0.5 and 0.8 mM at pH 7 under sunlight irradiation. Comparative degradation for the phenolic compounds is shown in Fig. 4b. The optimum phenolic compounds concentration is found at 0.5 mM. Around 95.3%, 97.3% and 98.3% degradation for phenol, 2-CP and 2-NP, respectively is obtained at pH 7 and phenolic concentration of 0.5 mM. The degradation efficiency of all the three compounds at various phenol concentrations is shown in Fig. S7. Catalyst loading on the photodegradation of phenolic compounds is studied in the range of 0.1–1 gL^{-1}. As the concentration of catalyst increases from 0.1 to 0.5 gL^{-1} through 0.3 gL^{-1}, the degradation efficiency of phenol gradually increase from 84.81% for phenol, 91.98% for 2-CP and 93.98% for 2-NP (using 0.1 gL^{-1}) to 95.3% for phenol, 97.3% for 2-CP and 98.3% for 2-NP (using 0.5 gL^{-1}). However, with increase in the catalyst concentration from 0.5 gL^{-1} to 0.8 gL^{-1} and then to 1 gL^{-1}, the photocatalytic degradation efficiency is found to be decrease. Using 1 gL^{-1} of catalyst concentration, the degradation efficiencies are found to be 83.12% for phenol, 86.29% for 2-CP and 88.28% for 2-NP which is much lower than the degradation efficiency using 0.5 gL^{-1} of catalyst concentration. This decrease of photocatalytic degradation efficiency of phenolic compounds with increase in the catalyst concentration is probably due to loss of active sites on the catalyst surface that leads to lower surface to volume ratio of the photocatalyst and hence lowers the degradation efficiency. A comparative figure showing the effect of catalyst loading is shown in Fig. 4c.

The photocatalytic degradation efficiency for all the three phenolic compounds i.e. phenol, 2-CP and 2-NP was also carried out in presence of P25 (Degussa TiO_2) and compared with that of Au-Pd/g-C_3N_4 and Au-Pd/rGO nanocomposites under sunlight irradiation. The comparative photocatalytic degradation efficiency of Au-Pd/rGO nanocomposites is already published in one of our earlier publication (Darabdhara et al., 2016). The experimental findings suggest good efficiency of our reported Au-Pd/g-C_3N_4 and Au-Pd/rGO photocatalyst with that of degussa TiO_2. Using degussa TiO_2, a semiconductor photocatalyst, degradation efficiency of around 95% was achieved for all the three phenolic compounds in 120 min and already reported in our earlier publication (Darabdhara et al., 2016). In presence of Au-Pd/g-C_3N_4 nanocomposite, degradation efficiency of 95.3%, 97.3% and 98.3% was obtained for phenol, 2-CP and 2-NP, respectively in 180 min. The comparative degradation efficiency is presented in Fig. S8 and Table S2. The comparative study suggest a good degradation rate for all the three phenolic compounds using our synthesized Au-Pd/g-C_3N_4 and is comparable with conventional degussa TiO_2 used for photocatalysis.

3.4. Comparative efficiency of photocatalytic degradation of Au-Pd/g-C_3N_4 in presence of sunlight and UV-light

Photocatalytic degradation of Au-Pd/g-C_3N_4 was investigated in presence of sunlight and UV light irradiation. Degradation efficiency of about 71.7%, 74.9%, 76.8% for phenol, 2-CP and 2-NP, respectively was achieved under UV light in 240 min whereas under similar reaction conditions, degradation efficiency of 95.3%, 97.3%, 98.3% for phenol, 2-CP and 2-NP, respectively was achieved under sunlight irradiation in 180 min. Comparative degradation profile using Au-Pd/g-C_3N_4 nanocomposite in presence of sunlight and UV light irradiation is shown in Fig. 4d. For the UV experiments, UV light of wavelength 254 nm and power 125 W was used for the purpose. All the experiments were performed in a manner similar to that performed in presence of sunlight irradiation. In presence of UV light, the degradation efficiency of Au-Pd/g-C_3N_4 nanocomposite was found to be lower in comparison to that in sunlight. It is because g-C_3N_4 has a greater tendency to absorb visible light than UV light. Moreover, Au nanoparticles also strongly absorbs visible light because of the surface plasmon resonance effect and also more than 43% of the solar energy is in the visible part of the spectrum and thus, Au-Pd/g-C_3N_4 nanocomposite exhibits better photocatalytic properties in presence of sunlight than that in UV light.

3.5. Comparative degradation of phenolic compounds in presence of sunlight and UV light using Au-Pd/rGO and Au-Pd/g-C_3N_4 nanocomposites

Investigation on the efficiency of support material rGO and g-C_3N_4 on the photocatalytic decomposition of phenolic compounds in presence of sunlight and UV-light is shown in Fig. S9a and S9b, respectively. Presence of g-C_3N_4 in the nanocomposites leads to increased photocatalytic efficiency both in presence of sunlight and UV light. In presence of sunlight, 95.3%, 97.3%, 98.8% for phenol, 2-CP and 2-NP, respectively was achieved using Au-Pd/g-C_3N_4 nanocomposite in just 180 min. On the other hand, 94.4% for phenol, 96.7% for 2-CP and 98.6% for 2-CP degradation was achieved using Au-Pd/rGO nanocomposite in 300 min. Similar observations was noticed under UV light. In presence of UV light, 71.7% for phenol, 74.9% for 2-CP and 76.8% for 2-NP degradation efficiency was obtained in 240 min using Au-Pd/g-C_3N_4 nanocomposite. In case of Au-Pd/rGO, degradation efficiency of 65.3%, 69.3% and 71.1% was achieved respectively for phenol, 2-CP and 2-NP in 300 min. Thus, it is observed that greater degradation efficiency is achieved using Au-Pd/g-C_3N_4 nanocomposite in less time whereas Au-Pd/rGO nanocomposite seems to be less efficient for degradation of organic pollutants. Due to the incorporation of nitrogen atoms in the carbon skeleton of g-C_3N_4, g-C_3N_4 gains much better properties then carbon based material rGO and thus behaves as a better photocatalyst (Fang et al., 2017). Clearly the role of support material towards degradation is well established. g-C_3N_4 with a band gap of 2.7 eV acts as an attractive visible light photocatalyst. Moreover, around 43% of the available solar energy accounts to visible light and due to the SPR effect, Au is capable of absorbing more visible light and so Au-Pd/g-C_3N_4 nanocomposite is capable of harvesting more visible light and thus acts as a better catalyst then Au-Pd/rGO nanocomposite towards degradation of phenolic compounds in water.

3.6. Kinetics of photocatalysis

Degradation of the phenolic compounds is found to follow Langmuir-Hinshelwood model given by

$$\ln (C_0/C) = kt \quad (1)$$

where, C_0 represents the initial phenol concentration, C is the concentration at a time t. A plot of ln (C_0/C) vs t (Fig. S10 (a-c)) gives a straight line, whose slope is obtained by linear regression and gives the rate constant of the first order reaction. Table S3 represents the rate constants and the linear regression coefficients of photodegradation of phenolic compounds under various phenolic concentrations.

3.7. Degradation mechanism

With a band gap of 2.7 eV, g-C_3N_4 exhibits typical semiconductor properties. Absorption of UV or visible light causes the excitation of an electron from the valence band (VB) to the conduction band (CB) resulting in the generation of holes (h^+) in the CB and electrons (e^-) in the corresponding VB. This e^- in VB initiates the oxidation processes for photocatalytic degradation. However, the generation of $e^- - h^+$ pair at the photocatalyst surface competes with the fast recombination rate of the charge carriers. This recombination decreases the photocatalytic efficiency. Several methods were adopted for designing the surface of g-C_3N_4 such as textural design, supramolecular chemistry, elemental doping, copolymerization etc. (Ong et al., 2016). Modification of g-C_3N_4 with noble metals is a promising method to broaden visible light absorption capacity (Mishra et al., 2012). Ways have been adopted to construct noble metal-semiconductor heterojunctions to obtain space-charge separation region also known as Schottky barrier. Such barriers results additional negative charges and positive holes in the noble metal and semiconductor respectively leading to sufficient suppression in the recombination. Additionally, noble metals because of their SPR can strongly absorb visible light leading to enhanced photocatalysis (Sarina et al., 2013). In a report by Pawar, Au nanoparticles increase the light absorption capacity of g-C_3N_4 resulting in increased photocatalytic activity (Pawar et al., 2015). Au nanoparticles because of SPR can considerably harvest visible light. Moreover, low Fermi level of Au nanoparticles results in transfer of electrons from the conduction band of g-C_3N_4 resulting in decreased recombination of the charge carriers. Also, the role of Pd nanoparticles is noteworthy. Chen et al. reported that Pd nanoparticles on g-C_3N_4 resulted in separation of photoinduced charge carriers leading to strong absorption in the visible light region (Chang et al., 2013). A combination of Au and Pd in the form of bimetallics on g-C_3N_4 may be used for better harvesting visible light from the solar spectrum due to the synergistic effects of both the metals resulting in decreased fermi level of the composite and possible lowering of the recombination rate of the photocatalytic charge carriers.

Absorption of photons by Au-Pd/g-C_3N_4 under light irradiation results in the transfer of e^- from the CB to the VB creating an electron deficiency or hole (h^+) in the VB and at the same time an electron (e^-) in the CB which is of oxidizing and reducing equivalents (Equation (2)). In aqueous suspension, h^+ generates hydroxyl (OH•) radicals (Equation (3)). Electrons (e^-) in the CB captures dissolved O_2 and generate $O_2^{\bullet-}$ (Equation (4)). This $O_2^{\bullet-}$ combine with H_2O to form OH• radicals (Equations (5)–(7)). These reactive species (h^+, $O_2^{\bullet-}$, OH•) can efficiently degrade phenol to intermediate products and finally to CO_2 and H_2O (Equation (8)).

$$\text{Au-Pd/g-}C_3N_4 + h\nu \rightarrow \text{Au-Pd/g-}C_3N_4\,(h^+ + e^-) \quad (2)$$

$$h^+ + H_2O \rightarrow H^+ + OH\bullet \quad (3)$$

$$O_2 + e- \rightarrow O_2-\bullet \quad (4)$$

$$O_2^{\bullet-} + H^+ \rightarrow \bullet OOH \quad (5)$$

$$\bullet OOH + H^+ + e^- \rightarrow H_2O_2 \quad (6)$$

$$H_2O_2 + e^- \rightarrow OH^\bullet + OH^- \quad (7)$$

$$h^+ + O_2^{\bullet -} + OH^\bullet + \text{phenolic compounds} \rightarrow \text{Intermediate products} \rightarrow CO_2 + H_2O \quad (8)$$

3.8. Hydroxyl radical formation

Since hydroxyl radical plays the major role in the degradation of organic pollutants, it is thus important to ascertain its presence and amount. The generation of the hydroxyl radicals was studied through photoluminescence (PL) analysis (Fig. 5). Typically, terephthalic acid (TA) acts as the probe molecule that can react with hydroxyl radical forming 2-hydroxyterepthalic acid (TAOH) which shows a fluorescent signal (Zhang et al., 2014). The excitation and the emission wavelengths were set at 315 nm and 410 nm, respectively. More the generation of hydroxyl radical, more intense is the fluorescence signal at 410 nm. For the PL analysis, 5 mg of all the g-C_3N_4 based composite catalyst was dispersed in an aqueous solution of TA/NaOH (1:2, mol/mol; 1×10^{-5} M) along with phenol solution (0.5 mM) and stirred in dark to study the adsorption-desorption equilibrium followed by exposure to natural sunlight. 3 mL sample solution was withdrawn at certain time interval and PL spectra were recorded. Fig. 5a represents the fluorescence spectra of all the composite catalyst and it is seen that Au-Pd/g-C_3N_4 nanocomposite demonstrates higher fluorescence signal which signifies the effectiveness of the nanocomposite in producing hydroxyl radical in the reaction mixture as compared to the monometallic nanocomposites. Fig. 5b represents the fluorescence signal of Au-Pd/g-C_3N_4 nanocomposite at different time intervals: 10, 30 and 180 min. It is observed that the intensity of the signal at 410 nm increases with increase in time interval thus indicating a linear increase of hydroxyl radical with increasing irradiation time.

3.9. Determination of final product of photodegradation

Chemical oxygen demand (COD) is also widely used as an efficient technique to determine the organic strength of wastewater i.e. it measures the oxygen equivalent of the organic content present in the sample which can be oxidized in presence of a strong oxidant to CO_2 and H_2O. In COD analysis, 3 mL of the phenol, 2-CP and 2-NP solutions were allowed to react with COD solution A (Merck, USA) and COD solution B (Merck, USA) and allowed to digest using a digestor, Spectroquant Pharo 300 spectrophotometer. The COD experiment was carried out using 0.5 mM initial phenol concentration and 0.5 gL^{-1} catalyst loading under sunlight irradiation. The degradation efficiency determined using the COD method is presented in Table S4 and are found to be 89.3, 92.3 and 94.1 for phenol, 2-CP and 2-NP, respectively. The COD results are in good agreement with the results of photocatalytic degradation using Au-Pd/g-C_3N_4.

The ion chromatography was used to determine the final products of degradation of 2-CP and 2-NP. The corresponding chloride (Cl^-) anion from 2-CP and nitrate anion (NO_3^-) from 2-NP was detected in anion chromatography at time 30, 120 and 180 min during the photocatalytic experiments. The ion chromatogram of 2-CP and 2-NP at different times during photocatalytic degradation is shown in Fig. S11. In the 2-CP solution subjected to sunlight irradiation (Fig. S11a), the peak for Cl^- ion was detected at 30 min and the intensity of this peak increased with time (Fig. S11b). At 180 min (Fig. S11c), the intensity of the peak was highest indicating the increase in the concentration of Cl^- with increased sunlight irradiation time. The appearance of the Cl^- ion in the solution is a clear evidence of degradation of the 2-CP molecule to its final product. The $OH^\bullet$ radical produced during the reaction oxidizes 2-CP to its corresponding acid and finally to CO_2, H_2O and Cl^- ion. Similarly for 2-NP, ion chromatogram was recorded at 30, 120 and 180 min (Fig. S11 (d-f)). The ion chromatogram of 2-NP at 30 min did not show presence of NO_3^- ion but with increasing irradiation time, the peak for NO_3^- ion appears at its intensity increases. At 210 min of sunlight irradiation, the signal for NO_3^- was strongest indicating the presence of a large number of these ions in the reaction mixture and excellent degradation of 2-NP.

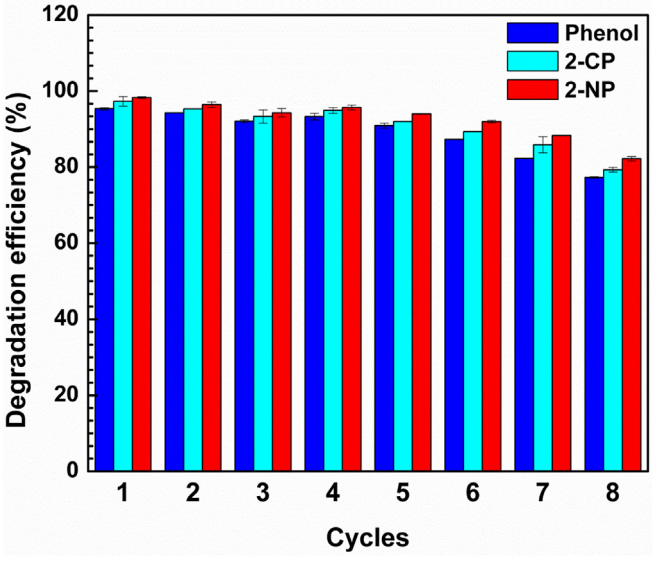

Fig. 6. Reusability of Au-Pd/g-C_3N_4 nanocomposite towards phenol, 2-CP and 2-NP at a phenol concentration of 0.5 mM, catalyst loading 0.5 gL^{-1} and pH 7.

3.10. Reusability and sustainability study of Au-Pd/g-C_3N_4 nanocomposite

Ascertaining the sustainability of the photocatalyst is an important key point. Thus, we analysed the reusability of Au-Pd/g-C_3N_4 after several cycles of reactions. The experiment was carried out under sunlight irradiation at a phenol concentration of 0.5 mM, catalyst loading 0.5 gL^{-1} and pH 7. After degradation, the photocatalyst was filtered and repeatedly washed with water and acetone and dried at 70 °C for 2 h for further cycles. Following this, the photocatalyst was mixed with fresh phenolic solution and degradation experiments continued up to eight consecutive cycles. About 95.35%, 97.3% and 98.3% degradation efficiency for phenol, 2-CP and 2-NP, respectively was obtained in the 1st cycle which decreased upto 77.28%, 79.28% and 82.19% for phenol, 2-CP and 2-NP, respectively in the 8th cycle. Thus, Au-Pd/g-C_3N_4 nanocomposite exhibit excellent reusability as shown in Fig. 6. The reusability of Au-Pd/g-C_3N_4 nanocomposite was compared to our previously reported Au-Pd/rGO nanocomposite. The Au-Pd/rGO nanocomposite exhibited degradation efficiency above 90% for the first four cycles and then tends to lose its activity in the 5th cycle. Thus, our newly synthesized Au-Pd/g-C_3N_4 nanocomposite exhibited better reusability towards the phenolic compounds in comparison to Au-Pd/rGO nanocomposite and thus is more sustainable in nature.

The changes associated with the crystallinity, surface morphology and size of the photocatalyst was studied by characterizing the composite after their photocatalytic activity with techniques such as XRD, TEM and FESEM (Fig. 7). The XRD analysis

of the Au-Pd/g-C_3N_4 nanocomposite was performed both before and after degradation of the phenolic compounds as shown in Fig. 7A. The XRD peaks for 2θ value of 39.24°, 45.60°, 66.66°, 80.32° and 84.60° corresponds to (111), (200), (220), (311) and (222) crystallographic planes of the Au-Pd/g-C_3N_4 nanocomposite. The peaks due to these planes of Au-Pd/g-C_3N_4 nanocomposite remain the same both before and after photocatalytic degradation of phenol. It is observed that there is not much change in the crystallinity of the nanocomposite. The TEM images of the Au-Pd/g-C_3N_4 nanocomposite after performing five consecutive cycles of photocatalytic degradation experiments and is represented in Fig. 7B. The medium magnification TEM images as in Fig. 7B (a) shows the presence of spherical bimetallic nanoparticles of Au-Pd on wrinkled and folded sheets of g-C_3N_4 with a size distribution of 47.3 nm (Fig. 7B (b)). The HRTEM image reveals the presence of crystal lattice corresponding to both Au and Pd. Lattice fringes corresponding to the (111) planes of Au and (200) planes of Pd face-centered cubic (*fcc*) structures with an interplanar spacing of 0.23 nm and 0.19 nm, respectively is seen in Fig. 7B (c). The SAED pattern also reveals the crystalline nature of the nanocomposite. It is clear from the TEM images that the nanocomposite retains the crystalline property even after performing five cycles of photocatalytic degradation experiments. Moreover, no noticeable change in the morphology and size distribution has been observed. The TEM images thus clearly reflect the stability of the photocatalyst. The FESEM images of Au-Pd/g-C_3N_4 nanocomposite after performing the photocatalytic reaction is shown in Fig. 7C which also clearly show that no significant change in the surface morphology of the nanocomposite.

4. Conclusions

Au-Pd/g-C_3N_4 nanocomposites was successfully designed by an eco-friendly technique and compared the photocatalytic performance with Au-Pd/rGO nanocomposite reported previously. For the first time, the Au-Pd/g-C_3N_4 and Au-Pd/rGO nanocomposites were used as active photocatalyst towards oxidation of carcinogenic phenolic compounds in water under both sunlight and UV-light. Encouraging results with more than 95% degradation was achieved for all the selected pollutants using Au-Pd/g-C_3N_4 nanocomposite in presence of sunlight in 180 min which is higher than many other reported photocatalysts. Also, the degradation efficiency of Au-Pd/g-C_3N_4 is higher than Au-Pd/rGO because incorporation of nitrogen atoms in the carbon skeleton of g-C_3N_4 provides much better properties than carbon based materials. g-C_3N_4 with a band gap of 2.7 eV acts as an attractive visible light

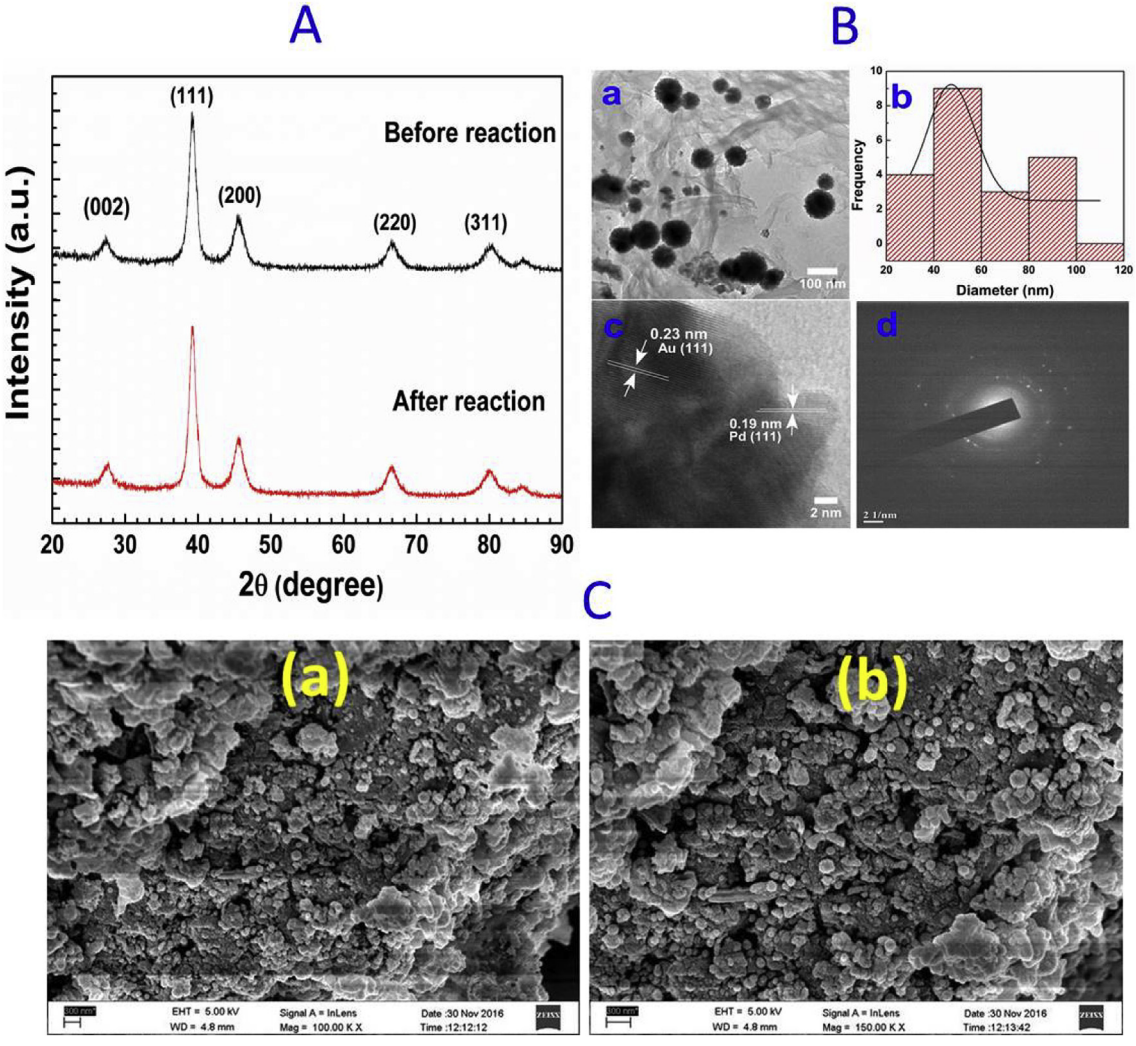

Fig. 7. (A) XRD pattern; (B) TEM Images: Medium magnification TEM image (a) Size distribution (b) HRTEM (c) SAED pattern (d) and (C) FESEM images of Au-Pd/g-C_3N_4 nanocomposite after reaction.

photocatalyst and since around 43% of the available solar energy accounts to visible light and due to the SPR effect Au is capable of absorbing more visible light so Au-Pd/g-C_3N_4 nanocomposite is capable of harvesting more sunlight and thus acted better then Au-Pd/rGO nanocomposite towards degradation of phenolic compounds. Photoluminescence results further revealed the efficient charge separation and delayed recombination of photo-induced electron-hole pairs in the Au-Pd/g-C_3N_4 nanocomposite. Generation of reactive oxygen species during photocatalysis is well explained through photoluminescence study and sustainability of these photocatalyst was ascertained through reusability study up to eight and five consecutive cycles for Au-Pd/g-C_3N_4 and Au-Pd/rGO nanocomposites, respectively without substantial loss in its activity which is much higher than any other reported nanocomposites. Characterization of the photocatalyst after reaction indicated no significant change in the size, crystallinity and morphology thus assuring its stability and sustainability. This work is believed to promote interest towards developing other such bimetallic nanoparticles on different 2D materials and exploring their potential in the field of photocatalysis as well as other sustainable applications.

Acknowledgements

The authors thank the CSIR, New Delhi for financial support (Project No. OLP-2003) and thankful to the Director, CSIR-NEIST, Jorhat for his interest to carry out the work. GD acknowledges DST, India for INSPIRE Fellowship. We thank the Advanced Analytical Facility for the FESEM facility and SAIF, NEHU, Shillong for the HRTEM facility. We also extend our thankfulness to Dr. Yumnam Silla from Biological Sciences and Technology Division of CSIR-NEIST for her help in carrying out the COD experiment.

Appendix A. Supplementary data

Supplementary data related to this article can be found at https://doi.org/10.1016/j.chemosphere.2018.01.073.

References

Akhavan, O., Ghaderi, E., 2009. Photocatalytic reduction of graphene oxide on TiO_2 thin film for photoinactivation of bacteria in solar light irradiation. J. Phys. Chem. C 113, 20214–20220.

Bai, X., Zong, R., Li, C., Liu, D., Liu, Y., Zhu, Y., 2014. Enhancement of visible photocatalytic activity via Ag@C_3N_4 core–shell plasmonic composite. Appl. Catal., B 147, 82–91.

Boukhatem, H., Khalaf, H., Djouadi, L., Gonzalez, F.V., Navarro, R.M., Santaballa, J.A., Canle, M., 2017. Photocatalytic activity of mont-La (6%)-$Cu_{0.6}Cd_{0.4}S$ catalyst for phenol degradation under near UV visible light irradiation. Appl. Catal., B 211, 114–125.

Cybula, A., Priebe, J.B., Pohl, M.-M., Sobczak, J.W., Schneider, M., Jurek, A.Z., Brückner, A., Zaleska, A., 2014. The effect of calcination temperature on structure and photocatalytic properties of Au/Pd nanoparticles supported on TiO_2. Appl. Catal. B 152–153, 202–211.

Chang, C., Fu, Y., Hu, M., Wang, C.Y., Shan, G.Q., Zhu, L.Y., 2013. Photodegradation of bisphenol A by highly stable palladium-doped mesoporous graphite carbon nitride (Pd/mpg-C_3N_4) under simulated solar light irradiation. Appl. Catal., B 142–143, 553–560.

Chen, D.M., Wang, K.W., Xiang, D.G., Zong, R.L., Yao, W.Q., Zhu, Y.F., 2014a. Significantly enhancement of photocatalytic performances via core-shell structure of ZnO@mpg-C_3N_4. Appl. Catal., B 147, 554–561.

Chen, L.C., Zeng, X.T., Si, P., Chen, Y.M., Chi, Y.W., Kim, D.H., Chen, G., 2014b. Gold-nanoparticle-graphite like C_3N_4 nanosheet nanohybrids used for electrochemiluminescent immunosensor. Anal. Chem. 86, 4188–4195.

Darabdhara, G., Amin, M.A., Mersal, G.A.M., Ahmed, E.M., Das, M.R., Zakaria, M.B., Malgras, V., Alshehri, S.M., Yamauchi, Y., Szunerits, S., Boukherroub, R., 2015. Reduced graphene oxide nanosheets decorated with Au, Pd and Au–Pd bimetallic nanoparticles as highly efficient catalysts for electrochemical hydrogen generation. J. Mater. Chem. A 3, 20254–20266.

Darabdhara, G., Boruah, P.K., Borthakur, P., Hussain, N., Das, M.R., Ahamad, T., Alshehri, S.M., Malgras, V., Wu, K.C.-W., Yamauchi, Y., 2016. Reduced graphene oxide nanosheets decorated with Au–Pd bimetallic alloy nanoparticles towards efficient photocatalytic degradation of phenolic compounds in water. Nanoscale 8, 8276–8287.

Deng, M., Yang, X., Silke, M., Qiu, W.M., Xu, M.S., Borghs, G., Chen, H.Z., 2011. Electrochemical deposition of polypyrrole/graphene oxide composite on microelectrodes towards tuning the electrochemical properties of neural probes. Sensor. Actuator. B Chem. 158, 176–184.

Diak, M., Klein, M., Klimczuk, T., Lisowski, W., Remita, H., Medynska, A.Z., Grabowska, E., 2017. Photoactivity of decahedral TiO_2 loaded with bimetallic nanoparticles: degradation pathway of phenol-1-13C and hydroxyl radical formation. Appl. Catal., B 200, 56–71.

D'Oliveira, J.C., Al-Sayyed, G., Pichat, P., 1990. Photodegradation of 2- and 3-chlorophenol in titanium dioxide aqueous suspensions. Environ. Sci. Technol. 24, 990–996.

Fang, W., Deng, Y., Tang, L., Zeng, G., Zhou, Y., Xie, X., Wang, J., Wang, Y., Wang, J., 2017. Synthesis of Pd/Au bimetallic nanopar ticle-loaded ultrathin graphitic carbon nitride nanosheets for highly efficient catalytic reduction of p-nitrophenol. J. Colloid Interface Sci. 490, 834–843.

Fageria, P., Uppala, S., Nazir, R., Gangopadhyay, S., Chang, C.-H., Bas, M., Pande, S., 2016. Synthesis of monometallic (Au and Pd) and bimetallic (AuPd) nanoparticles using carbon nitride (C_3N_4) quantum dots via the photochemical route for nitrophenol reduction. Langmuir 32, 10054–10064.

Feng, J.-J., Chen, L.-X., Song, P., Wu, X.-L., Wang, A.-J., Yuan, J., 2016. Bimetallic AuPd nanoclusters supported on graphitic carbon nitride: one-pot synthesis and enhanced electrocatalysis for oxygen reduction and hydrogen evolution. Int. J. Hydrogen Energy 41, 8839–8846.

Fujishima, A., Honda, K., 1972. Electrochemical photolysis of water at a semiconductor electrode. Nature 238, 37–38.

Ge, L., Zuo, F., Liu, J.K., Ma, Q., Wang, C., Sun, D.Z., Bartels, L., Feng, P., 2012. Synthesis and efficient visible light photocatalytic hydrogen evolution of polymeric g-C_3N_4 coupled with CdS quantum dots. J. Phys. Chem. C 116, 13708–13714.

Grabowska, E., Marchelek, M., Klimczuk, T., Lisowski, W., Zaleska-Medynska, A., 2016. Preparation, characterization and photocatalytic activity of TiO_2 microspheres decorated by bimetallic nanoparticles. J. Mol. Catal. Chem. 424, 241–253.

Han, C., Wu, L., Ge, L., Li, Y., Zhao, Z., 2015a. AuPd bimetallic nanoparticles decorated graphitic carbon nitride for highly efficient reduction of water to H_2 under visible light irradiation. Carbon 92, 31–40.

Han, C., Lu, Y., Zhang, J., Ge, L., Li, Y., Chen, C., Xin, Y., Wu, L., Fang, S., 2015b. Novel PtCo alloy nanoparticle decorated 2D g-C_3N_4 nanosheets with enhanced photocatalytic activity for H_2 evolution under visible light irradiation. J. Mater. Chem. A 3, 23274–23282.

Han, D.H., Cha, S.Y., Yang, H.Y., 2004. Improvement of oxidative decomposition of aqueous phenol by microwave irradiation in UV/H_2O_2 process and kinetic study. Water Res. 38, 2782–2790.

Kang, N., Lee, D.S., Yoon, J., 2002. Kinetic modeling of Fenton oxidation of phenol and monochlorophenols. Chemosphere 47, 915–924.

Keith, L., Telliard, W., 1979. ES & T Special Report: priority pollutants: I-a perspective view. Environ. Sci. Technol. 13, 416–423.

Liu, G., Niu, P., Sun, C.H., Smith, S.C., Chen, Z.G., Lu, G.Q., Chen, H.M., 2010. Unique electronic structure induced photoreactivity of sulfur-doped graphitic C_3N_4. J. Am. Chem. Soc. 132, 11642–11648.

Liu, M., Yin, X., Ulin-Avila, E., Geng, B., Zentgraf, T., Ju, L., Wang, F., Zhang, X., 2011. A graphene-based broadband optical modulator. Nature 474, 64–67.

Lin, Y.M., Dimitrakopoulos, C., Jenkins, K.A., Farmer, D.B., Chiu, H.Y., Grill, A., Avouris, P., 2010. 100-GHz Transistors from wafer-scale epitaxial graphene. Science 327, 662–662.

Low, J., Cao, S., Yu, J., Wageh, S., 2014. Two-dimensional layered composite photocatalysts. Chem. Commun 50, 10768–10777.

Mentin, O., Sun, X.L., Sun, S.H., 2013. Monodisperse gold–palladium alloy nanoparticles and their composition-controlled catalysis in formic acid dehydrogenation under mild conditions. Nanoscale 5, 910–912.

Mishra, Y.K., Chakravadhanula, V.S.K., Hrkac, V., Jebril, S., Agarwal, D.C., Mohapatra, S., Avasthi, D.K., Kienle, L., Adelung, R., 2012. Crystal growth behavior in Au-ZnO nanocomposite under different annealing environments and photoswitchability. J. Appl. Phys. 112, 064308/1–064308/5.

Nair, R.R., Blake, P., Grigorenko, A.N., Novoselov, K.S., Booth, T.J., Stauber, T., Peres, N.M., Geim, A.K., 2008. Fine structure constant defines visual transparency of graphene. Science 320, 1308.

Novoselov, K.S., Geim, A.K., Morozov, S.V., Jiang, D., Zhang, Y., Dubonos, S.V., Grigorieva, I.V., Firsov, A.A., 2004. Electric field effect in atomically thin carbon films. Science 306, 666–669.

Ong, W.-J., Tan, L.-L., Ng, Y.H., Yong, S.-T., Chai, S.-P., 2016. Graphitic carbon nitride (g-C_3N_4)-Based photocatalysts for artificial photosynthesis and environmental remediation: are we a step closer to achieving sustainability? Chem. Rev. 116, 7159–7329.

Padilla, R.H., Priecel, P., Lin, M., Lopez-Sanchez, J.A., Zhong, Z., 2017. A versatile sonication-assisted deposition–reduction method for preparing supported metal catalysts for catalytic applications. Ultrason. Sonochem. 35, 631–639.

Panigrahy, B., Sarma, D.D., 2015. Enhanced photocatalytic efficiency of AuPd nanoalloy decorated ZnO-reduced graphene oxide nanocomposites. RSC Adv. 5, 8918–8928.

Pawar, R.C., Khare, V., Lee, C.S., 2014. Hybrid photocatalysts using graphitic carbon nitride/cadmium sulfide/reduced graphene oxide (g-C_3N_4/CdS/RGO) for superior photodegradation of organic pollutants under UV and visible light. Dalton Trans. 43, 12514–12527.

Pawar, R.C., Lee, C.S., 2014. Single-step sensitization of reduced graphene oxide sheets and CdS nanoparticles on ZnO nanorods as visible-light photocatalysts.

Appl. Catal., B 144, 57–65.
Pawar, R.C., Pyo, Y., Ahn, S.H., Lee, C.S., 2015. Photoelectrochemical properties and photodegradation of organic pollutants using hematite hybrids modified by gold nanoparticles and graphitic carbon nitride. Appl. Catal., B 176–177, 654–666.
Pawar, R.C., Kang, S., Park, J.H., Kim, J.-H., Ahn, S., Lee, C.S., 2017. Evaluation of multi-dimensional hybrid photocatalyst for enrichment of H_2 evolution and elimination of dye/non-dye pollutants. Catal. Sci. Technol 7, 2579–2590.
Ren, H.-T., Jia, S.-Y., Wu, Y., Wu, S.-H., Zhang, T.-H., Han, X., 2014. Improved photochemical reactivities of $A_{g2}O$/g-C_3N_4 in phenol degradation under UV and visible light. Ind. Eng. Chem. Res. 53, 17645–17653.
Sarina, S., Waclawik, E.R., Zhu, H., 2013. Photocatalysis on supported gold and silver nanoparticles under ultraviolet and visible light irradiation. Green Chem. 15, 1814–1833.
Sharifian, H., Kirk, D.W., 1986. Electrochemical oxidation of phenol. J. Electrochem. Soc. 133, 921–924.
Su, R., Tiruvalam, R., He, Q., Dimitratos, N., Kesavan, L., Hammond, C., Lopez-Sanchez, A.J., Bechstein, A.R., Kiely, C.J., Hutchings, G.J., Besenbacher, F., 2012. Promotion of phenol photodecomposition over TiO_2 using Au, Pd, and Au-Pd nanoparticle. ACS Nano 6, 6284–6292.
Tahir, M., Cao, C., Mahmood, B.N., Butt, F.K., Mahmood, A., Idrees, F., Hussain, S., Tanveer, M., Ali, Z., Aslam, I., 2014. Multifunctional g-C3N4 nanofibers: a template-free fabrication and enhanced optical, electrochemical, and photocatalyst properties. ACS Appl. Mater. Interfaces 6, 1258–1265.
Tian, Y.L., Chang, B.B., Lu, J.L., Fu, J., Xi, F., Dong, X.P., 2013. Hydrothermal synthesis of graphitic carbon nitride-Bi_2WO_6 heterojunction with enhanced visible light photocatalytic activities. ACS Appl. Mater. Interfaces 5, 7079–7085.
Turchi, C.S., Ollis, D.F., 1990. Photocatalytic degradation of organic water contaminants: mechanisms involving hydroxyl radical attack. J. Catal. 122, 178–192.
Verma, S., Baig, R.B.N., Nadagouda, M.N., Varma, R.S., 2017. Hydroxylation of benzene via C–H activation using bimetallic CuAg@g-C_3N_4. ACS Sustain. Chem. Eng. 5, 3637–3640.
Wang, X.C., Maeda, K., Thomas, A., Takanabe, K., Xin, G., Carlsson, J.M., Domenet, K., Antonietti, M., 2009. Metal-free polymeric photocatalyst for hydrogen production from water under visible light. Nat. Mater. 8, 76–80.
Wang, X.C., Blechert, S., Antonietti, M., 2012. Polymeric graphitic carbon nitride for heterogeneous photocatalysis. ACS Catal. 2, 1596–1606.
Wei, T.Y., Wang, Y.Y., Wan, C.C., 1990. Photocatalytic oxidation of phenol in the presence of hydrogen-peroxide and titanium dioxide powders. J. Photochem. Photobiol., A 55, 115–126.
Wu, Z.-L., Ondruschka, B., Cravotto, G., 2008. Degradation of phenol under combined irradiation of microwaves and ultrasound. Environ. Sci. Technol. 42, 8083–8087.
Xiao, Q., Sarina, S., Jaatinen, E., Jia, J.F., Arnold, D.P., Liu, H.W., Zhu, H., 2014. Efficient photocatalytic Suzuki cross-coupling reactions on Au–Pd alloy nanoparticles under visible light irradiation. Green Chem. 16, 4272–4285.
Xu, M., Liang, T., Shi, M., Chen, H., 2013. Graphene-like two-dimensional materials. Chem. Rev. 113, 3766–3798.
Yao, F., Li, X., Wan, C., Xu, L., An, Y., Ye, M., Lei, Z., 2017. Highly efficient hydrogen release from formic acid using a graphitic carbon nitride-supported AgPd nanoparticle catalyst. Appl. Surf. Sci. 426, 605–611.
Yamamoto, Y., Niki, E., Shiokawa, H., Kamiya, Y., 1979. Ozonation of organic compounds. 2. Ozonation of phenol in water. J. Org. Chem. 44, 2137–2142.
Yang, S.B., Gong, Y.J., Zhang, J.S., Zhan, L., Ma, L.L., Fang, Z.Y., Vajtai, R., Wang, X., Ajayan, P.M., 2013. Exfoliated graphitic carbon nitride nanosheets as efficient catalysts for hydrogen evolution under visible light. Adv. Mater 25, 2452–2456.
Zhang, H., Gu, X., Liu, P., Song, J., Cheng, J., Su, H., 2017a. Highly efficient visible-light-driven catalytic hydrogen evolution from ammonia borane using non-precious metal nanoparticles supported by graphitic carbon nitride. J. Mater. Chem. A 5, 2288–2296.
Zhang, J., Lu, Y., Ge, L., Han, C., Li, Y., Gao, Y., Li, S., Xu, H., 2017b. Novel AuPd bimetallic alloy decorated 2D $BiVO_4$ nanosheets with enhanced photocatalytic performance under visible light irradiation. Appl. Catal. B Environ. 204, 385–393.
Zhang, N., Yang, M.-Q., Liu, S., Sun, Y., Xu, Y.-J., 2015. Waltzing with the versatile platform of graphene to synthesize composite photocatalysts. Chem. Rev. 115, 10307–10377.
Zhang, Y., Zhang, N., Tang, Z.-R., Xu, Y.-J., 2014. Graphene oxide as a surfactant and support for in-situ synthesis of Au–Pd nanoalloys with improved visible light photocatalytic activity. J. Phys. Chem. C 118, 5299–5308.
Zheng, Y., Liu, J., Liang, J., Jaroniec, M., Qiao, S.Z., 2012. Graphitic carbon nitride materials: controllable synthesis and applications in fuel cells and photocatalysis. Energy Environ. Sci. 5, 6717–6731.